



## Microgrooving of a single-crystal diamond tool using a picosecond pulsed laser and some cutting tests

Nozomi Takayama, Jun Ishizuka, Jiawang Yan\*

Department of Mechanical Engineering, Keio University, Hiyoshi 3-14-1, Kohoku, Yokohama, Kanagawa 223-8522, Japan



### ARTICLE INFO

**Keywords:**  
 Laser processing  
 Micromachining  
 Single-crystal diamond  
 Groove formation  
 Metal cutting  
 Functional surface  
 Structured surface

### ABSTRACT

Irradiation of a single-crystal diamond tool was performed with a picosecond pulsed laser to produce a tool with a microgrooved edge. This tool was then used in a metal cutting process to transfer the edge grooves onto a workpiece. Suitable conditions for laser irradiation on the diamond tool were experimentally investigated in terms of groove shape and laser-induced damage to diamond. Two different kinds of cutting experiments were performed; a uniformly grooved surface and a hierarchically structured surface were obtained. The chip formation mechanisms in the metal grooving process were examined. A copper workpiece was rapidly machined the surface of which had microgrooves with a pitch of a few micrometers. An increase of the contact angle was observed on the grooved surface, indicating the improvement of water repellency. This study presents an efficient method to machine microgrooves on metal materials for functional surfaces.

### 1. Introduction

In recent years, microgrooves have become an increasingly useful surface structure in a wide range of applications. For example, microgrooves have been shown to improve cell alignment, enabling the growth of well-orientated cells for use in tissue repair [1]. In addition, these elongated cells are less adhesive and can be removed from the substrate easily [2]. This increases the survival rate of cultivated cells. They may also protect cells from the detrimental effects of fluidic shear stress and thus allow for the cultivation of sensitive cells [3]. Another example of microgroove use is to control surface wettability. Water repellent surfaces are needed in a broad spectrum of air-cooling applications. Water retention is problematic as it causes a reduction in the air-side heat transfer coefficient, a greater core pressure drop and bacterial growth [4]. Microgrooved surfaces would greatly increase the efficiency of a cooling system. Furthermore, water repellent surfaces are shown to have self-cleaning properties, as water drops will easily roll off the surface [5,6]. A third use for microgrooves can be found in the field of bionics [7,8]. The grooving of implants is particularly difficult as the implant surface is normally curved, and a large surface area needs to be machined. As microgrooves are highly important surface structures, a method to machine them at high efficiency needs to be established.

There are various methods to machine microgrooves, but in order to obtain high form accuracy and low surface roughness, ultraprecision cutting is often used. Moreover, by using a tool servo system or a

piezoelectric vibration system to drive a cutting tool, the cutting of microgrooves on three-dimensional shapes, hierarchical structures and complex curved surfaces is possible. However, if the cutting of individual grooves with extremely small pitches is attempted, using a sharp single-point diamond tool, the machining time will become very long and the production cost very high. This would make it difficult to machine large areas.

One possible way to reduce machining time is to use a specially shaped tool with a grooved edge. Multiple grooves on the tool cutting edge would be transferred to the workpiece simultaneously during cutting. In this way, the side flow of workpiece material taking place in individual groove cutting will be suppressed, so that precise groove profiles will be generated without burr formation. However, to make the implementation of this method possible, it is necessary to establish a process to machine microgrooves on the tool. Single-crystal diamond (SCD) is often used as a tool material in ultraprecision cutting. Thus a method to groove SCD is needed.

As an extremely hard and brittle material, SCD cannot be grooved using conventional mechanical methods. Nonconventional machining methods such as focused ion beam machining (FIB) or reactive ion etching (RIE) have been attempted in recent years. FIB uses the collision energy of accelerated ions in order to remove material. It is not only expensive but also has a low material removal rate. This makes it unsuitable for the processing of large areas, such as a long cutting edge. RIE uses ions from a plasma to etch the SCD. This requires a complex and expensive system in order to induce the plasma. RIE is difficult to

\* Corresponding author.

E-mail address: [yan@mech.keio.ac.jp](mailto:yan@mech.keio.ac.jp) (J. Yan).

generate curved or slanted surfaces, like V-grooves. In addition, it often results in a high surface roughness due to the ions aggressively interacting with the surface [9]. Thus an alternative method is needed.

SCD can be processed using a pulsed laser [10–14]. The advantages of laser processing are that is relatively low cost, rapid and has high shape controllability. By using a short pulse width, it becomes possible to reduce the heat affected zone (HAZ), which refers to the region where thermal effects are observed, and unwanted phenomena such as thermal stress, material structure change and cracking take place. Irradiation diamond by a nanosecond pulse causes the formation of an amorphous carbon layer with an average thickness of  $\sim 2\text{ }\mu\text{m}$  and a HAZ with an average thickness of  $\sim 2.5\text{ }\mu\text{m}$  [15]. Some researchers have shown that femtosecond laser machining can be used to drill deep holes in diamond with high shape accuracies [16]. However, a femtosecond laser may result in the problem of intense laser beam self-focusing inside diamond [17]. This is caused by beam filamentation where light propagates through a medium without diffraction, causing self-focusing. Self-focusing produces non-homogeneous graphitized structures, in the form of irregular globules, and therefore deteriorates the machining quality [18]. This effect is lessened for pulse widths longer than 3 ps. From this point of view, a picosecond pulsed laser may be a more suitable choice to machine diamond with limited damage.

A few studies have used lasers to create micro-patterns on the rake face of a tool to reduce cutting force and temperature [19]. The patterns decrease the tool-chip contact area on the rake face. In addition, when the patterns are filled with a solid lubricant, a film forms during cutting and serves as a lubricating film. Micro-arrays have also been machined on diamond to enhance thermal and mechanical performance [20]. Thus, laser irradiation has been shown to be an effective method to improve the performance of SCD tools. However, no attempt has yet been made to machine microgrooves on the cutting edge of an SCD tool.

By using an SCD tool with patterned cutting edge on a commercially available diamond turning machine equipped with a high-speed air bearing spindle to rotate the workpiece, the grooving time for a large-area workpiece can be dramatically reduced compared with the use of a single-point tool. In addition, it becomes possible to machine complex cross-sectional shapes, such as V-grooves, grooves with curved and hierarchical cross sections on a metal workpiece.

Hierarchical grooves have several advantages over uniform grooves. Firstly, they can reduce drag to a greater extent than a uniform structure. An example of this is a bird feather. A feather possesses ripples on its surface; the heights of these ripples decrease towards the edge, creating a hierarchical structure. When compared to a uniform structure, the feather's structure results in a greater drag reduction rate [21]. Secondly, hierarchical structures can also be used to direct fluid flow. Kang et al. reported that uniform grooves are not capable of inducing a directional oil sliding property, so hierarchical grooves are necessary to create directional oil flow [22]. Additionally, hierarchical grooves are not perpendicular to the original surface of the workpiece unlike uniform grooves. This allows for control the color of the metal surface without changing the groove period or size. When light is incident on the grooved surface, a certain wavelength of light is reflected [23]. At different cutting edge angles, different wavelengths of light are reflected, thus altering the surface color and absorption properties of the surface. Not only does this have an aesthetic use, but a practical one such as in solar cell applications were structures are used to enhance ultraviolet absorptivity.

The objective of this study is to investigate the possibility of microgrooving an SCD tool by picosecond laser irradiation and using the grooved tool to establish an efficient method for cutting microgrooves on large-area metal surfaces. By using a picosecond pulse width, it might be possible to reduce the laser-induced damage to the diamond tool cutting edge. In the following experiments, the laser irradiation of an SCD tool was carried out. Then the tool was used in cutting experiments to investigate the possibility of transferring microgrooves from the cutting edge to the metal workpiece surface in an

**Table 1**  
Laser parameters.

Laser type	Fibre laser
Wavelength [nm]	1030
Pulse width [ps]	50, 800
Repetition rate [kHz]	100, 300, 1000
Spot size [ $\mu\text{m}$ ]	6 $\times$ 7
Laser fluence [J/cm <sup>2</sup> ]	4.5, 15.3, 18.5, 26.4, 49.4
Energy distribution	Gaussian

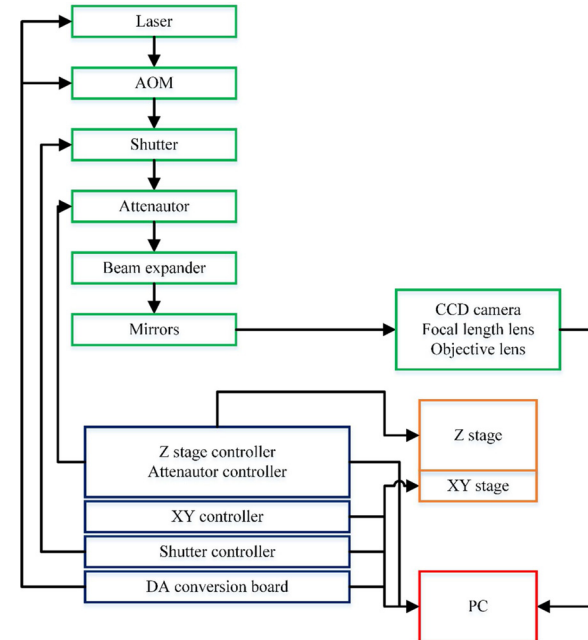


**Fig. 1.** Schematic of the laser controller system used.

ultraprecision cutting process.

## 2. Experimental method

The laser used was PFLA-1030TP made by Optoquest Co., Ltd, which incorporates a fiber laser. Irradiation was performed in ambient atmosphere using the parameters shown in Table 1. The laser controller system and the optical system are shown in Figs. 1 and 2, respectively. The laser spot is an ellipse. The laser used has an asymmetric active region and retains this ellipticity throughout the system. Thus the focused spot is also non-circular. The lens used to focus the laser beam onto the stage was M Plan Apo NIR 20X made by Mitutoyo Co. It has a NA of 0.4, and a focal length of 10 mm. The M2 size is  $< 1.4$ .

Laser processing was performed on a straight edge SCD tool as indicated in Fig. 3a. The laser was positioned so that the beam center was on the tool cutting edge and the beam was focused onto the rake face of

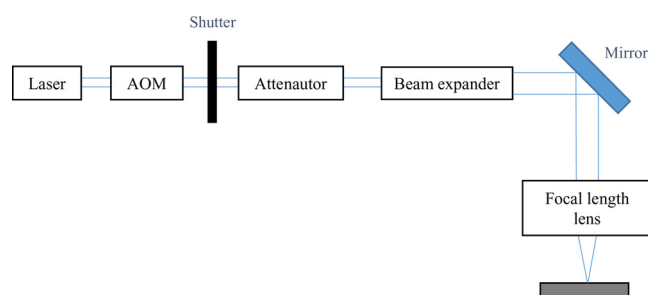


**Fig. 2.** Schematic of the optical system used.

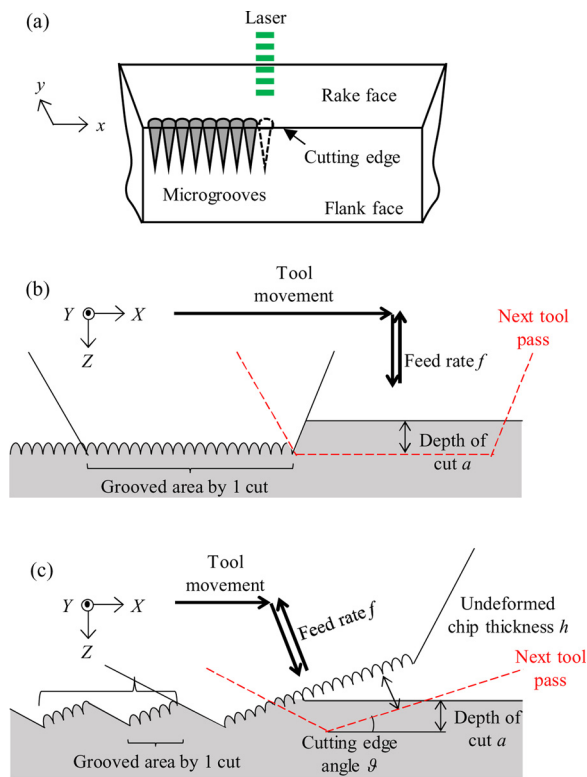


**Fig. 3.** Model of the machining method: (a) laser microgrooving of the tool followed by (b) uniform groove cutting and (c) cutting of a hierarchical surface structure with the microgrooved tool.

the tool. The laser beam is combined with a CCD camera which has the same focal point. This means that when the CCD camera is focused on a given surface, the laser is vertically focused onto the surface as well. The CCD camera was focused onto the rake face of the tool using a 1 axis-controlled stage for the z-direction so that the laser could be vertically focused. Then, as the center of the CCD image is also the center of the laser beam, the cutting edge was moved using a 2-axis controlled stage for the x and y directions, so that the edge was aligned at the center of the image. Stationary irradiation was performed, then the tool was moved 6  $\mu\text{m}$  in the x-direction and irradiation was repeated.

First, as a preliminary experiment to investigate the effect of pulse width, trial irradiation was performed on the cutting edge using a pulse width of 50 ps and 800 ps. Laser ablation is possible at a pulse width of 10 ns; as both pulse widths are shorter than 10 ns, it is assumed that laser ablation will occur [24]. Then, to determine the effect of repetition rate, trial plane irradiation was performed on an SCD chip, which had dimensions of 3 mm  $\times$  3 mm  $\times$  1.1 mm, with varying rates. Repetition rate would likely affect the amount of debris produced; therefore, to make the difference in debris accumulation obvious by irradiating a large area, plane irradiation was used. Then, various laser fluences were used to determine the most suitable value. Using the optimal values for repetition rate, pulse width and fluence, the entire cutting edge was irradiated for microgrooves.

Then, the grooved tool was used in a cutting experiment, as indicated in Figs. 3b and c, on a copper workpiece with a 20 mm diameter. The microgrooves had a maximum programmed depth of cut of 9  $\mu\text{m}$ . An ultraprecision diamond turning lathe Precitech Nanoform X (AMETEK Precitech Inc., USA), which also has a slow tool servo system, was used. The spindle rotation rate was 2700 rpm. The feed rate was 500 nm/rev in the Z-direction as shown in Fig. 4.

Two different surface structures were attempted. First, a uniformly grooved surface was cut, where the cutting edge is parallel to the workpiece surface as shown in Fig. 3b. A single tool contact produced a

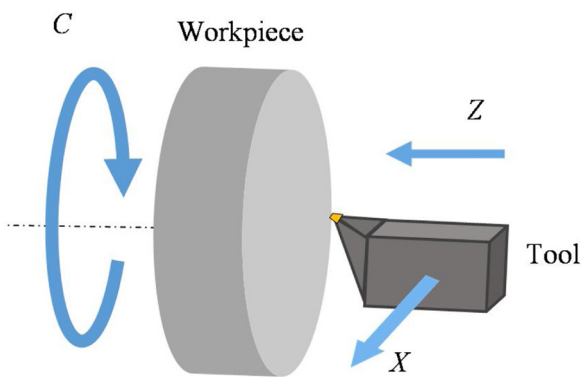


**Fig. 4.** Schematic of the cutting process.

grooved area with a width of 1.1 mm. This way, a large grooved area can be machined rapidly. The cutting experiments were performed under a dry condition and a wet condition using kerosene coolant. The tool contacted the workpiece 1 time during the experiment under dry conditions and 4 times in each of the experiments under wet conditions. Next, the machining of a hierarchical structured surface was attempted as shown in Fig. 3c. The tool came into contact with the workpiece at a cutting edge angle of 2°. This enabled the machining of hierarchical grooves; the surfaces of large grooves were covered in smaller microgrooves. Three cutting experiments were performed: one under a dry condition and two under wet conditions using kerosene coolant. The tool contacted the workpiece 1 time during the experiment under dry conditions and 4 times in each of the experiments under wet conditions. A single tool contact produced a grooved area with a width of 264  $\mu\text{m}$  with 40 grooves. The total machining time for the cutting process was roughly 5 min.

The tool before and after cutting, cutting chips and the cut copper surface were observed by a digital microscope VHX-1000 made by KEYENCE Corporation and Inspect S50 Scanning Electron Microscope (SEM) made by FEI Company. The surface structure of the cut copper and the tool was observed using a white light interferometer TalySurf CCI1000 made by Taylor Hobson Co., Ltd. and a laser probe unit MP-3 made by Mitaka Kohki Co., Ltd. The crystal structure was determined by Raman spectroscopy using a laser micro-Raman spectrometer NRS-3100 (JASCO Corporation). The contact angle of the surface was measured by SImage Entry 5 made by Excimer Inc.

### 3. Results and discussion

#### 3.1. Effect of pulse width

First, the effect of different laser pulse widths was investigated. Irradiation was performed at a constant laser fluence of 4.5 J/cm<sup>2</sup>, a constant repetition frequency of 100 kHz while two pulse widths, 50 ps and 800 ps, were used. When considering pulse width, it is important to consider the thermal diffusion length. The thermal diffusion length  $L$ , the distance that temperature change propagates during a single pulse width so the temperature is reduced by 1/e, can be calculated by the following Eq. (1).

$$L = (\alpha \times t_0)^{\frac{1}{2}} \quad (1)$$

where  $\alpha$  is the thermal diffusivity of diamond and  $t_0$  is the pulse width [25]. The thermal diffusion length of a 50 ps pulse is 125 nm and for an 800 ps pulse, it is 500 nm. Moreover, as SCD is a transparent material at the wavelength used, the optical penetration depth must also be considered. In considering the two parameters, thermal diffusion length and optical penetration depth, Konov states that when the pulse width is less than 100 ps, the laser-graphitized layer (and thus the HAZ) is thought to be characterized by the optical penetration depth, while for

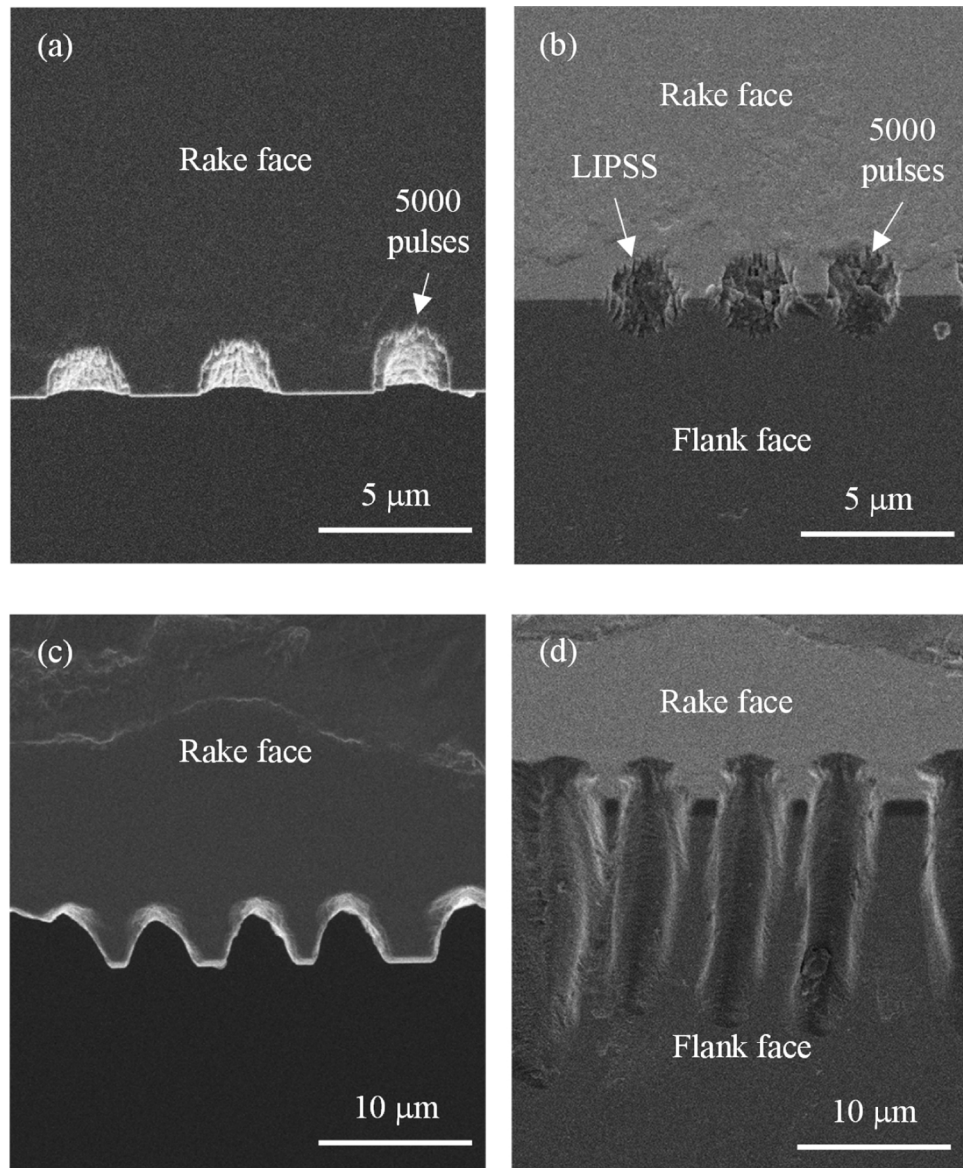


**Fig. 5.** SEM images of the cutting edge irradiated by varying pulse widths: (a) 50 ps observed from the rake face and (b) from an angle of 45° to the cutting edge, (c) 800 ps observed from the rake face and (d) from an angle of 45° to the cutting edge.

pulse widths greater than 100 ps, it is characterized by the thermal diffusion length [17]. It is known that machining takes place via diamond transformation into a graphitic phase. The optical penetration depth of graphite is 50 nm [17]. Therefore, theoretically, a shorter pulse has a much smaller HAZ compared to a longer pulse.

Irradiation of 5000 pulses was performed on the tool cutting edge using the 2 pulse widths. As shown in Fig. 5a, irradiation with 5000 pulses at a pulse duration of 50 ps did not result in sufficient material removal and the resulting grooves are very shallow. Under this condition, laser-induced periodic surface structures (LIPSS) can be seen in the edge areas of the irradiated spots shown in Fig. 5b. These LIPSS are thought to be caused by interference between the incident laser and the surface scattered wave related to the electrons excited by laser irradiation [26]. If LIPSS are present on the walls of the tool grooves, this high surface roughness will be transferred to the workpiece during cutting. In comparison, machining with 800 ps pulse produced deep and clear grooves with smooth surfaces. For this reason, a pulse width of 800 ps was employed in the following experiments.

It was noticed that no cracks were present on the rake face despite the brittle nature of SCD. This assumed to be because thermal

conduction into bulk diamond was limited by the short pulse as shown by Eq. (1), reducing thermal damage. The thermal diffusion length,  $L$ , is much smaller than the groove depth on the flank face so the heat affected zone is negligible. As heat affected zones are considerably weaker than un-damaged diamond, a small  $L$  ensured that the tool would maintain its hardness, and in turn, its service life.

### 3.2. Effect of repetition rate

Next, the effect of different repetition rates was investigated. Irradiation was performed at 100 and 1000 kHz, maintaining constant parameters for laser power (1.40 W) and scanning speed (1 mm/s). Raman spectroscopy was performed on a flat area 6 μm from the plane edge. These 2 repetition rates were chosen as a previous study involving simulations of laser irradiation showed that 1000 kHz causes significant thermal accumulation while 100 kHz results in none [27]. Without any thermal accumulation, the diamond is able to return to its original temperature (i.e. room temperature) after each laser pulse, limiting the formation of a heat affected zone. By comparing the two repetition frequencies, Fig. 6 shows that irradiation with 100 kHz results in a

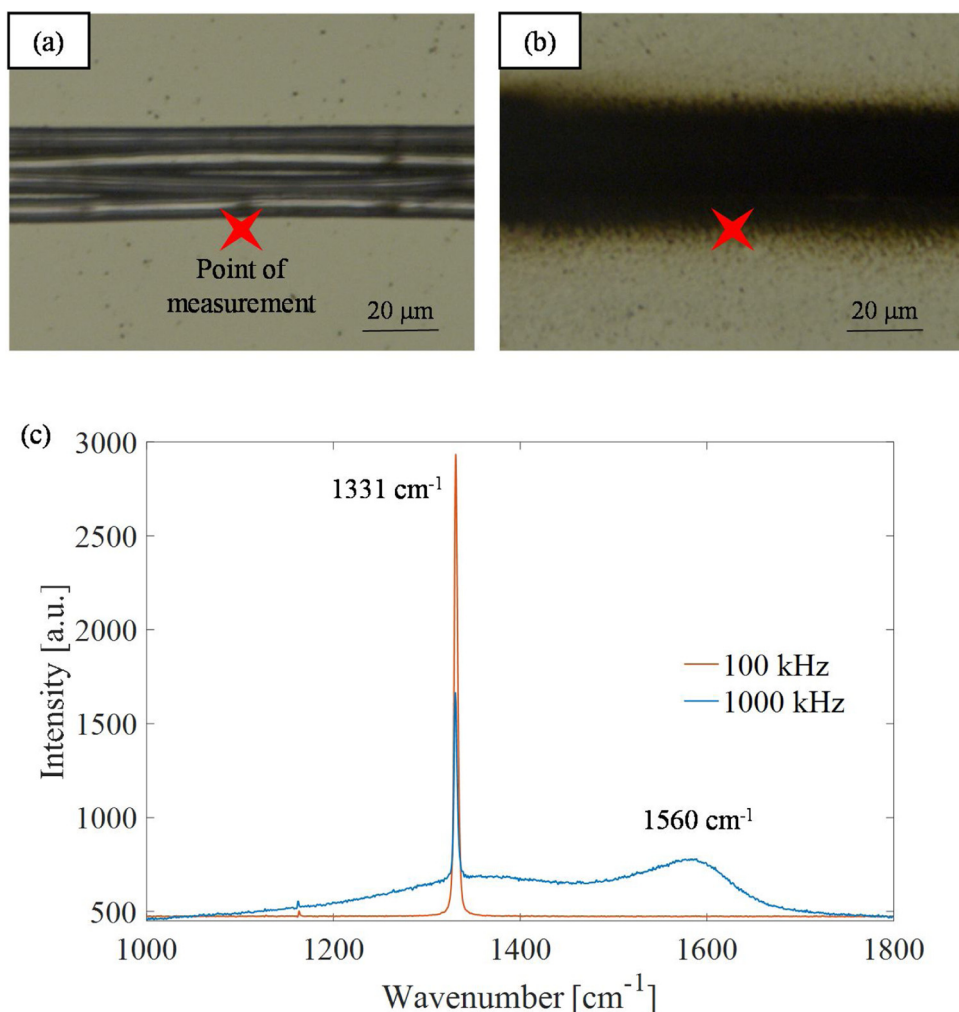


**Fig. 6.** Microscope images showing measured area when irradiation is performed at: (a) 100 kHz, (b) 1000 kHz and (c) the Raman spectra of each area.

**Table 2**

Effect of laser parameters on laser-induced graphitization and groove formation.

		Diamond graphitization	Microgroove depth	LIPSS formation
Pulse width	Long	Significant	Deep	No
	Short	Insignificant	Shallow	Yes
Repetition frequency	Low	Insignificant	–	–
	High	Significant	–	–

stronger diamond peak at 1331 cm<sup>-1</sup> than 1000 kHz, while 1000 kHz results in a stronger graphitic peak at 1560 cm<sup>-1</sup> than 100 kHz. Greater repetition rates are thought to induce greater graphitization due to thermal accumulation effects. As the time interval between consecutive pulses is shorter, the irradiated material has less time to cool, thus reaching a greater maximum temperature with each consecutive pulse. As graphitization occurs at around 900 K in air, this limited cooling and elevated temperature leads to increased graphitic debris production. As the formation and deposition of graphite is unwanted in the processing of the cutting edge, a lower frequency of 100 kHz was employed in the following experiments. The effects of both pulse width and repetition

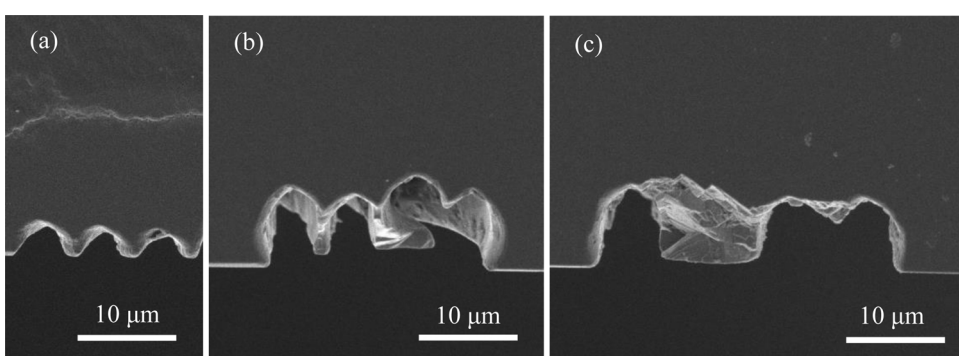


**Fig. 7.** SEM images of the cutting edge irradiated by varying fluences showing the rake face: (a) 15.3, (b) 18.5, (c) 26.4 J/cm<sup>2</sup>.

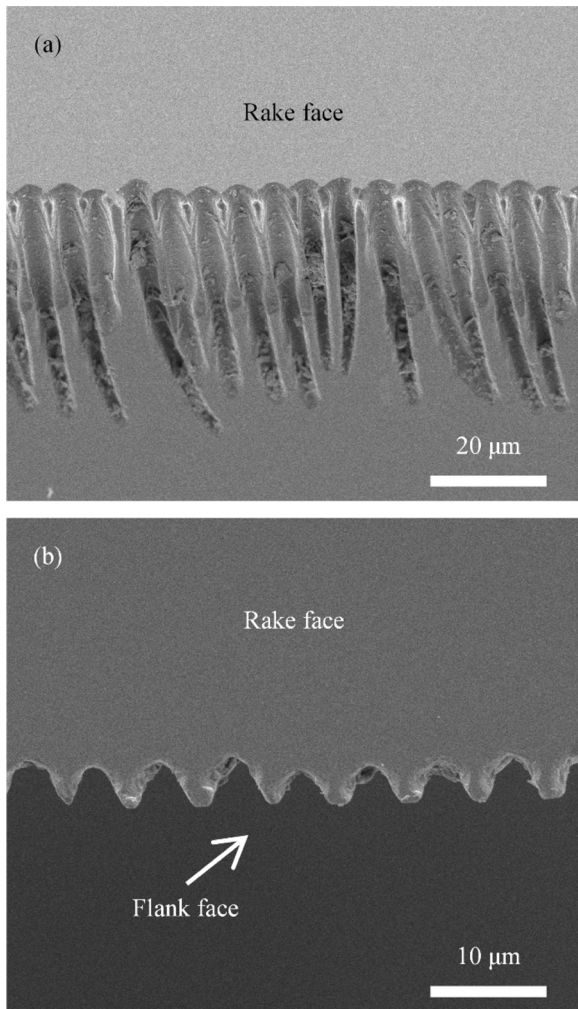


**Fig. 8.** SEM images of the grooved tool from (a) the flank face and (b) the rake face.

frequency on laser-induced graphitization are summarized in Table 2.

### 3.3. Effect of laser fluence

Next, experiments were conducted to determine the most suitable values for laser fluence. A pulse width of 800 ps was used. The SEM images of resulting grooves are shown in Fig. 7. The groove depths were over 20 μm for all fluences; for irradiation at 15.3 J/cm<sup>2</sup>, the depths of the grooves are roughly 25 μm. On the other hand, using large fluences of 18.5 J/cm<sup>2</sup> and 26.4 J/cm<sup>2</sup> resulted in cracking in a large zone (Figs. 7b and c). Moreover the grooves merged together and an uneven shape was obtained. Therefore in the subsequent experiments, a laser fluence of 15.3 J/cm<sup>2</sup> was employed.

### 3.4. Laser microgrooving of cutting edge

The tool was laser-irradiated to produce grooves on the cutting edge using 800 ps pulse width, 100 kHz repetition rate, 15.3 J/cm<sup>2</sup> laser fluence, 5000 pulses; the SEM images are shown in Fig. 8. The depth of the grooves ranged from 3–5 μm. The groove length ranged from 24–46 μm; the majority of the grooves had a length of ~40 μm. The dimensional variation may also be due to self-focusing properties in the bulk material. Self-focusing caused the generation of irregular graphitic structures, but this effect is less pronounced for pulses longer than 3 ps [17]. As diamond is a transparent material at the laser wavelength used, laser machining mainly commences from impurities, crystal defects and

micro-cracks [28]. Therefore, the size and depth of irradiation points depend on the distribution of such material aberrations. As the defect distribution is random, the resulting grooves have various depths and lengths.

In addition, some long grooves were shown to bend in random directions when observed from the flank face. This may be due to laser-induced diamond graphitization and crack formation in diamond. During the initial pulses, high pressures and temperatures are generated within the absorbing micro-cracks, leading to their propagation and widening. At the same time, laser irradiation causes the heating of diamond and its subsequent graphitization. Graphite is strongly absorbing over a large range of wavelengths, including infrared. Therefore, after graphitization, the graphite itself absorbs laser to reach a high temperature. Due to this large localized temperature gradient, high thermal stress is present, causing the material to crack [29]. The amount of graphite generation and the cracking of graphite is not dependent on the cleavage plane of diamond. As a result, the cracks propagate in random directions. After a crack is formed, the area surrounding the crack is preferentially heated, graphitized and machined. This is thought to produce the random bending of the grooves on the flank face, as shown in Fig. 8.

### 3.5. Metal cutting with the grooved tool

The workpiece was observed and measured after the cutting experiments. The grooves were successfully transferred from the grooved tool onto the copper workpiece as shown by the microscope image of Fig. 9. The groove edges are uneven under dry conditions. However, they are even under wet conditions and each groove can be clearly distinguished.

Next, the cross-sectional profiles of the grooves were measured, as presented in Fig. 10. It was found that the surface machined under dry conditions was more uneven compared to machining under wet

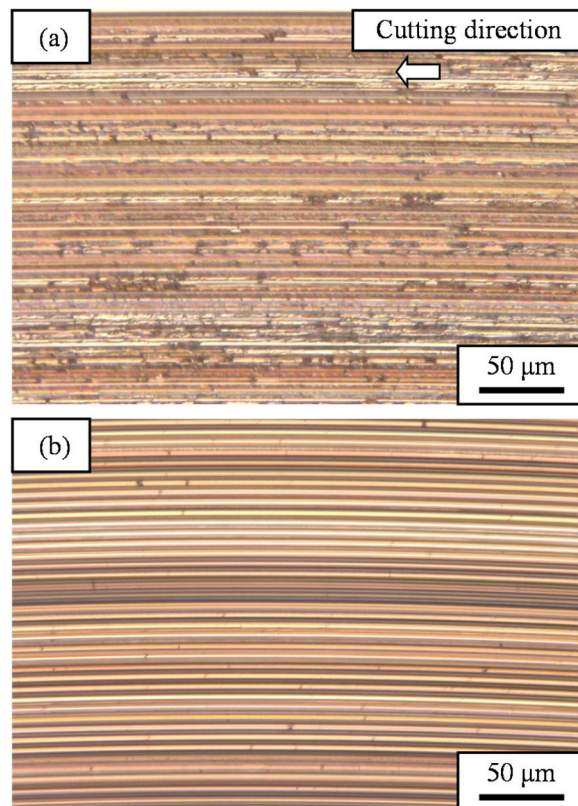


**Fig. 9.** Microscope image of the uniformly grooved copper workpiece cut under (a) dry conditions and (b) wet conditions.

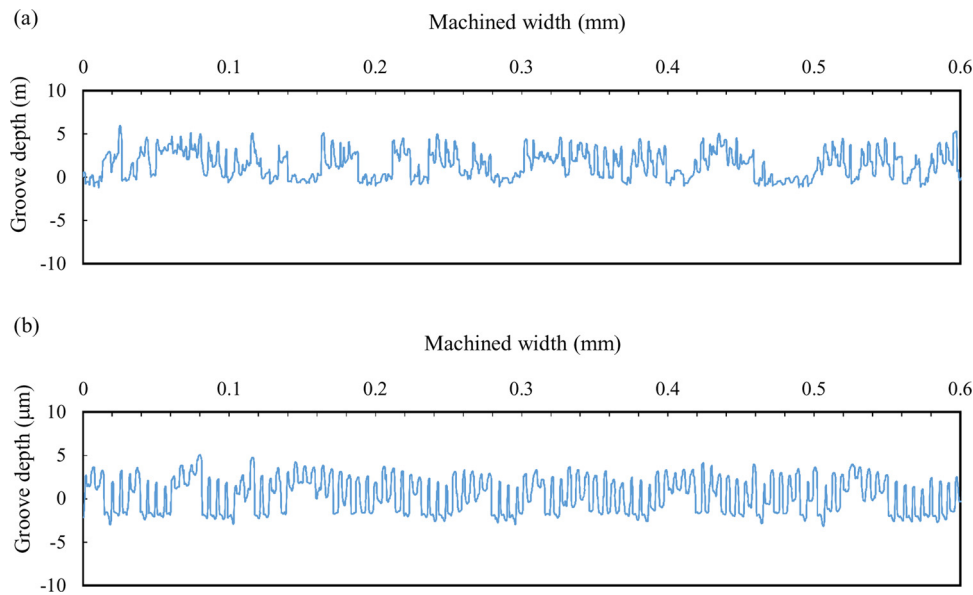


**Fig. 10.** Cross-sectional profiles of the grooves under (a) dry and (b) wet conditions.

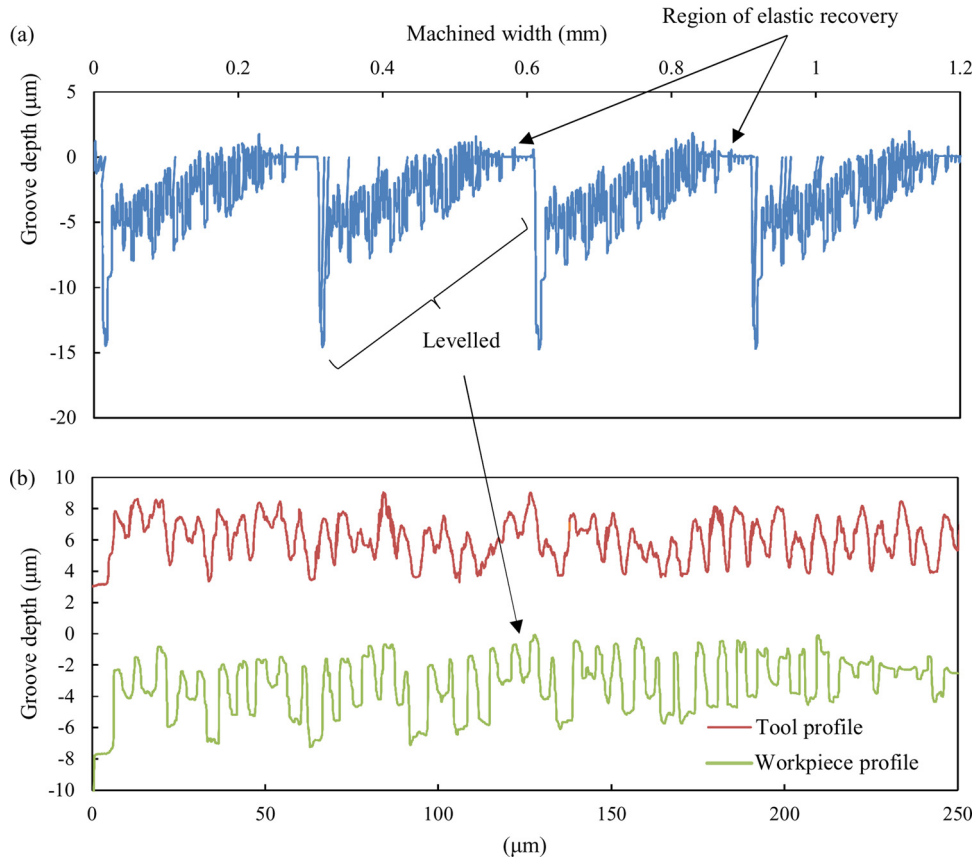


**Fig. 11.** Cross-sectional profiles of the grooves showing: (a) the hierarchical grooves and (b) the micron level grooves on the tool and the copper workpiece where the workpiece profile has been levelled.

conditions. There are sections where the grooves have not clearly been transferred to the workpiece in dry cutting.

With regards to hierarchical groove cutting, the results in Fig. 11 demonstrate that it is possible to easily machine hierarchical structures by using a grooved tool on a diamond turning machine. The profile of the entire machined area during one cutting test under wet conditions is shown in Fig. 11a. This profile shows the micron level grooves are generated on the diagonal surfaces of ten-micron level deep grooves. It

is noticed that some micron level grooves where the depth of cut approaches zero are not clearly machined. This may be attributed to the elastic recovery of workpiece material. At an extremely small depth of cut, the effect of elastic recovery becomes relatively significant.

The cross-sectional profile of the grooves on the copper workpiece was compared with the initial cutting edge profile. Here, the shape deformation will be considered in depth. As presented in Fig. 11b, the grooves machined onto the copper workpiece have a similar width and

height as the irradiated grooves on the cutting edge. However, the grooves on the workpiece surface are more rectangular compared to those on the tool. This means that the groove width at the base is constant but the width towards the groove peak is greater. The two sets of grooves were compared in detail. The height error is defined as below, where  $h_w$  is the groove height of the workpiece and  $h_t$  is the groove height of the cutting edge.

$$\text{Height error} = \frac{h_w - h_t}{h_t} \quad (2)$$

The width error is defined as below, where  $w_w$  is the groove width of the workpiece and  $w_t$  is the groove width of the cutting edge. Both width were measured at the base of the grooves.

$$\text{Width error} = \frac{w_w - w_t}{w_t} \quad (3)$$

The average height error was found to be  $20 \pm 6\%$ . This means that the groove heights on the workpiece surface were roughly 1.2 times larger than those on the cutting edge surface. The average width error was found to be  $2.4 \pm 0.8\%$ . Thus the average height error was greater than the average width error.

This shape deformation is thought to be due to contact between the workpiece surface and the flank face during the cutting process. After the grooves are generated by the tool rake face, the grooves will be slightly bended by the grooves on the flank face of the tool. This is because the grooves on the tool flank face are straight whereas those on the workpiece are curved due to the workpiece rotation in a face turning process. Contact on the flank face caused the groove to deform and the groove height to increase. Therefore, it is possible that the groove height increased within the bent part of the tool groove. This can also explain why there is greater height error compared to width error. This contact between the workpiece surface and the flank face is more likely to affect the groove peaks as they are more elevated compared to the rest of the machined surface and thus are more likely to contact the tool's flank face. In order to machine grooves with a given dimension, it is necessary to consider and compensate for the dimensional error. The secondary groove deformation is especially significant when the microgrooves on the tool flank face are long and the relief angle of the tool is small. In order to reduce the groove deformation, it is necessary to use a large relief angle and/or reduce the length of the microgrooves on the tool flank face. It should be pointed out that the secondary groove deformation will not occur in shaping and planning processes.

Moreover, by comparing the three-dimensional topographies of cut surfaces under various conditions shown in Fig. 12, it was confirmed that cutting under dry conditions produced uneven grooves. Again, this may be because of contact between the tool and workpiece. Moreover, the friction/adhesion is higher than in cutting with a non-grooved tool due to an increased contact area between the grooved tool and the copper workpiece. Friction and adhesion cause higher surface temperatures and significant material flow, resulting in a low surface integrity. Furthermore, cutting chips may have been trapped in the grooves, and scraped along the groove tops, leading to greater deformation. Use of a coolant improved the surface quality, as shown in Fig. 12b and d, as it reduced friction/adhesion and promoted the ejection of cutting chips.

In addition, in the cutting of hierarchical structures, burr formation can also be observed at the shoulder of the tool-workpiece contact area. The mechanism of this burr formation has been made clear by Asakura et al. [30] and is shown to be dependent on the cutting method. As the tool moves into the workpiece, squeezing effects arise at the sides of the tool and significant side burrs are generated. Burr formation may also be instigated by the cutting edge roundness change caused by laser machining; the cutting edge radius is likely to have increased after laser irradiation.

### 3.6. Tool wear

The cutting edge before and after cutting was compared to check for tool wear. The SEM image of the grooved edges after cutting is shown in Fig. 13. Although the groove surfaces have become slightly smoother after cutting compared with the edge before cutting as shown in Fig. 8b, there was no apparent tool wear or micro chipping. This is thought to be because of a limited heat affected zone forming during laser irradiation. The cutting edge mostly retained its original SCD properties such as high hardness and resistance to wear [17,30,31]. This shows that it is possible to use the tool multiple times. Furthermore, due to tool contact, it is possible that the graphitic debris formed on the cutting edge during laser machining was removed during metal cutting. Thus the groove tops appear cleaner after cutting.

### 3.7. Chip formation mechanism

Next, the cutting chips were observed and the SEM images of the chips produced during uniform groove cutting are shown in Fig. 14. Two types of chips were observed; Fig. 14a shows a thin flow type chip, where the chip width is several micrometres, while Fig. 14c shows a wide ( $\sim 200 \mu\text{m}$  in width) flat chip with thin cracks. The different types were thought to be due to whether the cutting edge grooves were filled or not. As indicated by Fig. 15, the chip formation mechanism can be described in three steps of a single plunge cut model. In the case where the grooves were not filled shown in Fig. 15a, or at the initial step of the cutting process, material removal only occurs at the protruding parts or the peaks of the cutting edge. Thus, thin chips are obtained. Their widths should and do correspond with the width of the tool's groove peaks. On the other hand, as cutting proceeds and the grooves begin to be filled (Fig. 15b and c), material removal occurs along the entire cutting edge. Thus, the wide chips are obtained. The running cracks are thought to be due to the chip becoming very thin at the deepest point or the curve of the groove. As the cutting depth increases as in Fig. 15a–c, the chip shape changed from those in Fig. 14a–c. Similar chips were obtained during the cutting of the hierarchical grooves.

### 3.8. Contact angle change at surface

The contact angles of the original and cut workpiece surface (machined under wet conditions) were measured. A droplet of  $2.6 \mu\text{L}$  pure water was used in a static sessile drop method. The droplet was observed from a direction parallel and perpendicular to the groove direction, referred to as Directions 1 and 2 in Fig. 16. The results are summarized in Table 3. Fig. 17 shows the photographs of the water droplet on the hierarchical grooved surface. The contact angle observed by both directions of both machined surfaces increased compared with that before cutting. No significant difference was observed between uniform and hierarchical grooves. Theoretically, the gravitational force acting when a water droplet is on the hierarchical groove is larger compared to the uniform groove. However, as the size of the water droplet used is small, the gravitational force has a smaller influence due to scaling effects. This may be the reason for similar contact angle for both surface structures.

A drop can normally stick to a given rough hydrophobic surface in one of two ways. It either sits on the peaks of the roughened areas or it fills the grooves (referred to as wetted contact) [32]. In the first case, the apparent contact angle can be given by Cassie's formula, if an isotropic surface is assumed [33]. In the second case, it can be given by the Wenzel equation [34]. If the surface geometry is anisotropic (not uniform in all directions), it has been reported that the contact angle along and perpendicular to parallel grooves is different [35]. This has been confirmed in this study as well.

Firstly, the contact angles obtained from the grooved surfaces from both directions are greater than the intrinsic contact angle ( $78.2^\circ$ ) due to squeezing of the droplet base. This squeezing effect is possibly due to

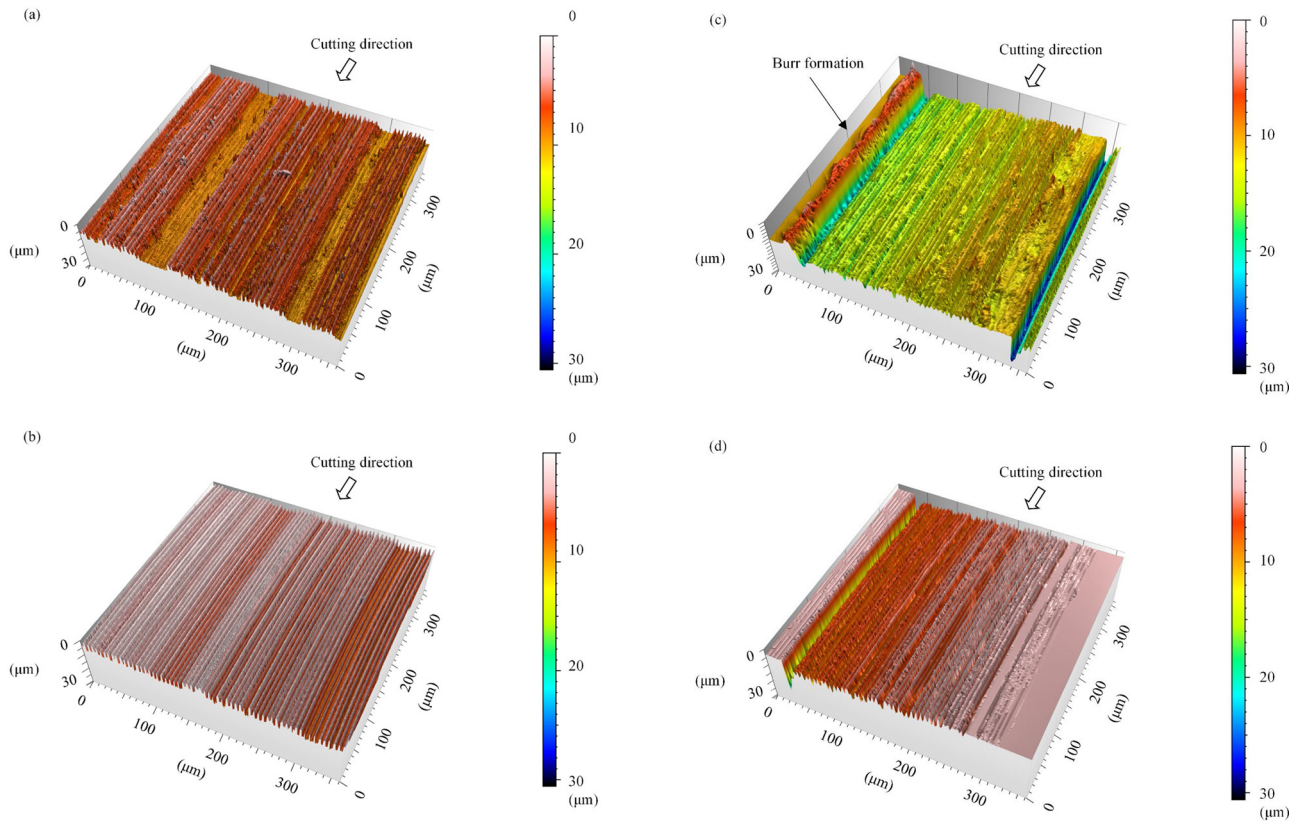


**Fig. 12.** Three-dimensional surface topographies of the copper workpiece: uniform grooves under (a) dry conditions and (b) wet conditions, and hierarchical surface under (c) dry conditions and (d) wet conditions.

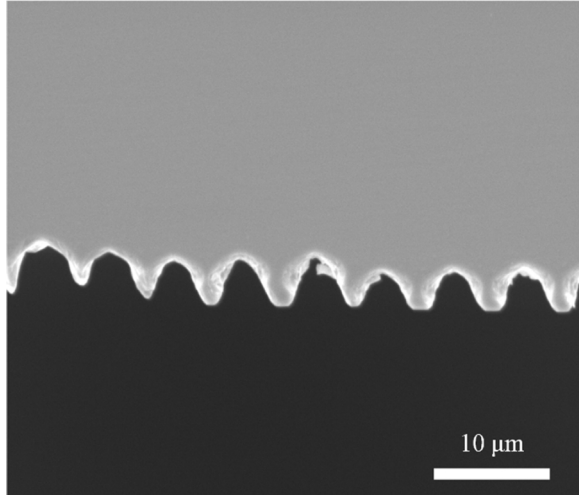


**Fig. 13.** SEM images of the grooved cutting edge after cutting.

the grooves forming a discontinuous, periodic distribution of surface energy [4]. This distribution results in the pinning of the contact line of the droplet base onto the edge of a given pillar until the groove can be bridged and the droplet spreads in a stick-slip manner. Additionally, due to this squeezing effect, the droplet is stretched favorably in Direction 2, in order to accommodate the volume. The spreading of the droplet is continuous in Direction 2 while it is discrete in Direction 1. Thus the droplet is elongated and its contact angle larger in Direction 2. The contact angle of Direction 2 remains greater than the intrinsic value due to the presence of air [36]. From previous studies of microgrooved surfaces, droplets in the Cassie state had a more spherical shape and droplet elongation is known to be significantly lower than droplets in

the Wenzel regime [37]. Therefore, it is possible to conclude that the droplets in this study are in the Cassie state; they reside on the peaks of the grooves, supported by air pockets between the grooves.

In general, the formation of hierarchical structures produces superhydrophobic states with contact angles of over  $150^\circ$  [38]. However, in our study, there was no apparent difference in the contact angle for the uniform and hierarchical grooves. Zhang et al. have also shown that some hierarchical structures do not produce an enhanced contact angle compared to a uniform structure [39]. This effect is thought to arise when the cosine of the intrinsic contact angle has a value close to zero. As a result, the roughness factor will have a minimal effect on the contact angle and no improvement will be observed. In such cases, Zhang et al. have suggested that may be possible to further increase the water repellency of the surface by changing the microgroove alignment. In this study, the major focus has been placed on the feasibility of efficient fabrication of hierarchical grooves, and their optimal design and surface property will be investigated in detail in the future.

#### 4. Conclusions

This study presents the possibility of grooving a cutting edge of a single-crystal diamond tool by a pulsed laser and using the grooved tool for metal cutting. The following conclusions were obtained from this study.

- A diamond tool was successfully microgrooved using a picosecond pulsed laser using a fluence of  $15.3 \text{ J/cm}^2$  and a repetition rate of 100 kHz. These conditions provided rapid machining without edge cracking and with limited graphite deposition.
- The two types of grooved surfaces, uniform and hierarchical, were successfully machined onto the copper workpiece with the grooved cutting edge. Reduced burr formation was obtained under wet conditions. Some shape transference error was observed due to

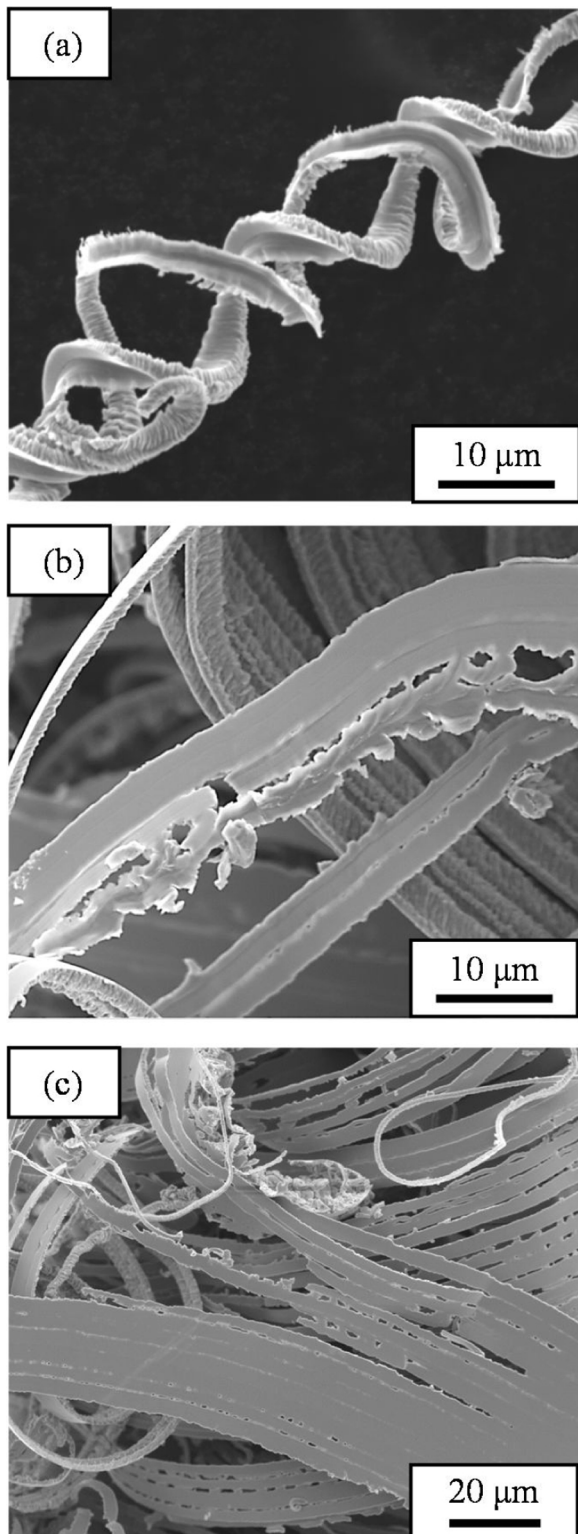


**Fig. 14.** SEM images of chips obtained from the uniform groove cutting process under wet conditions: (a) a chip formed when the groove is not filled by the workpiece, (b) partially filled by the workpiece, (c) completely filled by the workpiece.

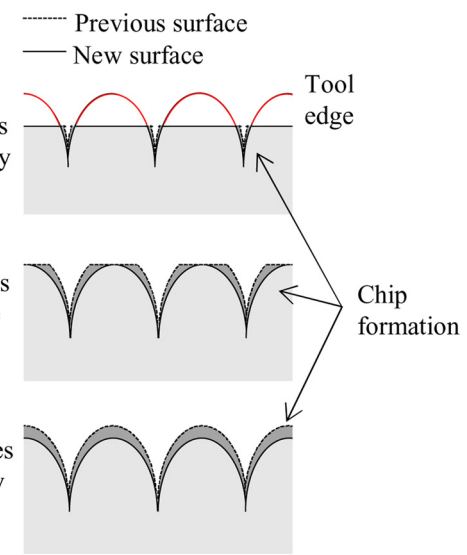
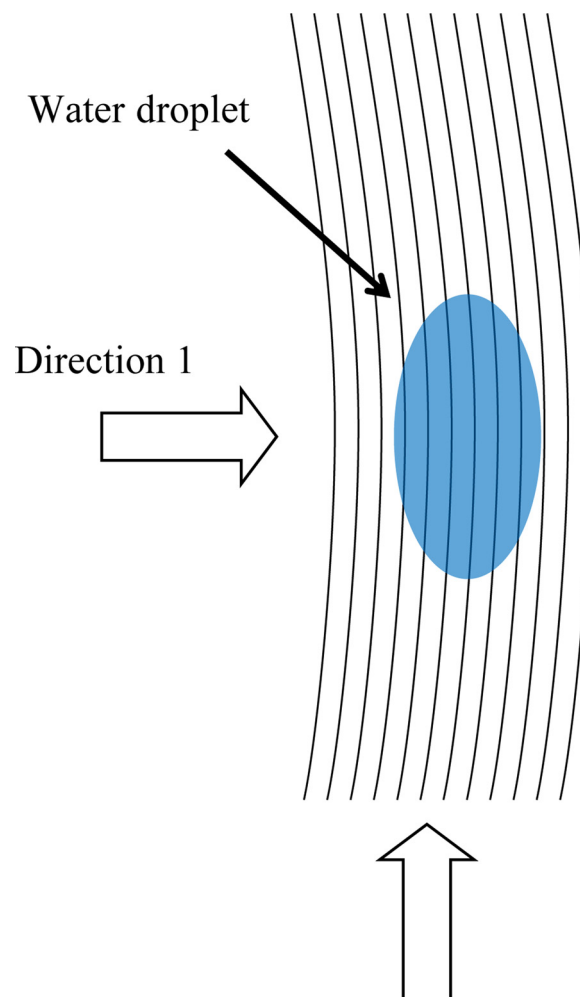


**Fig. 15.** Model of chip formation during a single plunge cut with a grooved tool.



**Direction 2**

**Fig. 16.** Schematic showing the observation direction during contact angle measurement.

material side flow during the cutting process.

- Two types of chips were observed, formed depending on whether the tool grooves were filled or not.
- The microgrooves resulted in contact angle increase from 78.2° to up to 123.9° and the formation of a water repellent surface.

**Table 3**  
Contact angle measurements.

		Contact angle (°)	Error (°)
Uniform grooves	Surface before machining	78.2	± 2.9
	Direction 1	123.9	± 3.0
	Direction 2	84.5	± 1.6
Hierarchical surface	Direction 1	122.1	± 2.6
	Direction 2	85.8	± 6.1

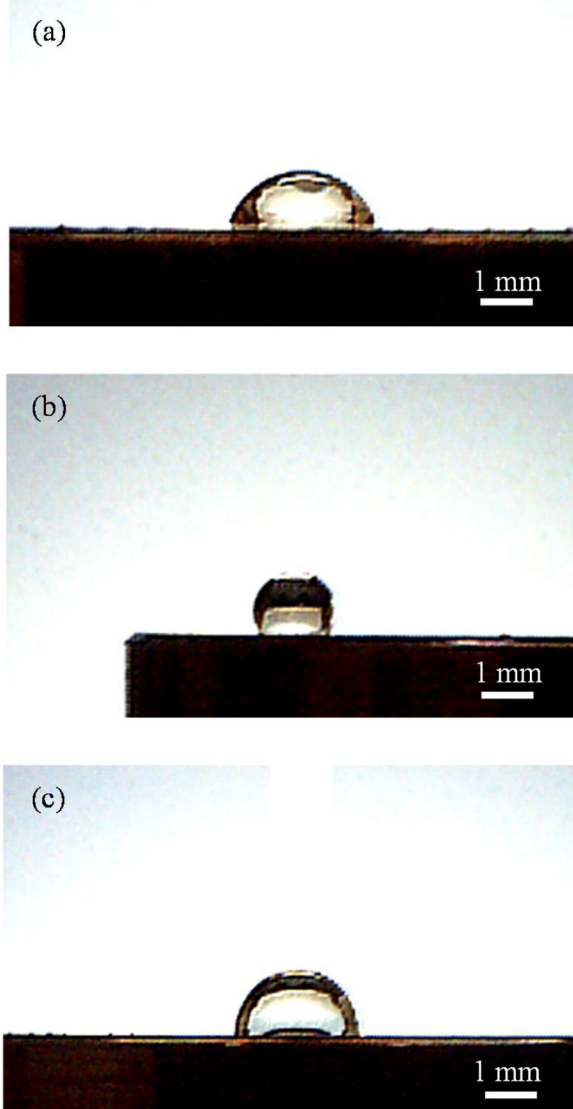


**Fig. 17.** Photographs showing the water droplet on: (a) the copper workpiece surface before machining, (b) the hierarchical surface after machining observed from direction 1, (c) from direction 2.

Future investigations will attempt to improve the laser micro-grooving process so that higher-precision grooves can be produced, to consider different groove shapes and to measure the tool life.

## References

- Wilkinson CDW, Riehle M, Wood M, Gallagher J, Curtis ASG. The use of materials patterned on a nano- and micro-metric scale in cellular engineering. *Mater Sci Eng C* 2002;19:263–9.
- Casey BG, Monaghan W, Wilkinson CDW. Embossing of nanoscale features and environments. *Microelectron Eng* 1997;35:393–6.
- Korin N, Bransky A, Khouri M, Dinnar U, Levenberg S. Design of well and groove microChannel bioreactors for cell culture. *Biotechnol Bioeng* 2009;102:1222–30.
- Sommers AD, Jacobi AM. Creating micro-scale surface topology to achieve anisotropic wettability on an aluminum surface. *J Micromech Microeng* 2006;16:1571–8.
- Barthlott W, Neinhuis C. Purity of the sacred lotus, or escape from contamination in biological surfaces. *Planta* 1997;202:1–8.
- Patankar NA. Mimicking the lotus effect: influence of double roughness structures and slender pillars. *Langmuir* 2004;20:8209–13.
- Qu J, Chehroudi B, Brunette DM. The use of micromachined surfaces to investigate the cell behavioural factors essential to osseointegration. *Oral Dis* 1996;2:102–15.
- Fasasi AY, Mwenifumbo S, Rahbar N, Chen J, Li M, Beye AC, et al. Nano-second UV laser processed micro-grooves on Ti6Al4V for biomedical applications. *Mater Sci Eng C* 2009;29:5–13.
- Pypen CMJM, Plenk H, Ebel MF, Svagera R, Wernisch J. Characterization of microblasted and reactive ion etched surfaces on the commercially pure metals niobium, tantalum and titanium. *J Mater Sci Mater Med* 1997;8:781–4.
- Mathis A, Courvoisier F, Froehly L, Furfar L, Jacquot M, Lacourt PA, et al. Micromachining along a curve: femtosecond laser micromachining of curved profiles in diamond and silicon using accelerating beams. *Appl Phys Lett* 2012;101:99–102.
- Rehman ZU, Janulewicz KA. Structural transformation of monocrystalline diamond driven by ultrashort laser pulses. *Diam Relat Mater* 2016;70:194–200.
- Konenko TV, Komlenok MS, Pashinin VP, Pimenov SM, Konov VI, Neff M, et al. Femtosecond laser microstructuring in the bulk of diamond. *Diam Relat Mater* 2009;18:196–9.
- Dumitru G, Romano V, Weber HP, Sentis M, Marine W. Femtosecond ablation of ultrahard materials. *Appl Phys A Mater Sci Process* 2002;74:729–39.
- Windholz R, Molian PA. Nanosecond pulsed excimer laser machining of chemical vapour deposited diamond and highly oriented pyrolytic graphite Part I An experimental investigation. *J Mater Sci* 1997;32:4295–301.
- Eberle G, Jefimovs K, Wegener K. Characterisation of thermal influences after laser processing polycrystalline diamond composites using long to ultrashort pulse durations. *Precis Eng* 2015;39:16–24.
- Ramanathan D, Molian P a. Micro- and sub-micromachining of type IIa single crystal diamond using a Ti:sapphire femtosecond laser. *J Manuf Sci Eng* 2002;124:389–96.
- Konov VI. Laser in micro and nanoprocessing of diamond materials. *Laser Photonics Rev* 2012;6:739–66.
- Konenko TV, Meier M, Komlenok MS, Pimenov SM, Romano V, Pashinin VP, et al. Microstructuring of diamond bulk by IR femtosecond laser pulses. *Appl Phys A Mater Sci Process* 2008;90:645–51.
- Jianxin D, Ze W, Yunsong L, Ting Q, Jie C. Performance of carbide tools with textured rake-face filled with solid lubricants in dry cutting processes. *Int J Refract Met Hard Mater* 2012;30:164–72.
- Butler-Smith PW, Axinte DA, Daine M. Preferentially oriented diamond micro-arrays: a laser patterning technique and preliminary evaluation of their cutting forces and wear characteristics. *Int J Mach Tools Manuf* 2009;49:1175–84.
- Chen H, Rao F, Shang X, Zhang D, Hagiwara I. Biomimetic drag reduction study on herringbone ripples of bird feather. *J Bionic Eng* 2013;10:341–9.
- Kang SM, Lee C, Kim HN, Lee BJ, Lee JE, Kwak MK, et al. Directional oil sliding surfaces with hierarchical anisotropic groove microstructures. *Adv Mater* 2013;25:5756–61.
- Ahsan MS, Ahmed F, Kim YG, Lee MS, Jun MBG. Colorizing stainless steel surface by femtosecond laser induced micro/nano-structures. *Appl Surf Sci* 2011;257:7771–7.
- Butler-Smith PW, Axinte DA, Pacella M, Fay MW. Micro/nanometric investigations of the effects of laser ablation in the generation of micro-tools from solid CVD diamond structures. *J Mater Process Technol* 2013;213:194–200.
- Zahedi A, Tawakoli T, Azarhoushang B, Akbari J. Picosecond laser treatment of metal-bonded CBN and diamond superabrasive surfaces. *Int J Adv Manuf Technol* 2015;76:1479–91.
- Wu Q, Ma Y, Fang R, Liao Y, Yu Q, Chen X, et al. Femtosecond laser-induced periodic surface structure on diamond film. *Appl Phys Lett* 2003;82:1703–5.
- Eaton S, Zhang H, Herman P, Yoshino F, Shah L, Bovatsek J, et al. Heat accumulation effects in femtosecond laser-written waveguides with variable repetition rate. *Opt Express* 2005;13:4708–16.
- Bloembergen N. Role of cracks, pores, and absorbing inclusions on laser induced damage threshold at surfaces of transparent dielectrics. *Appl Opt* 1973;12:661–4.
- Vouagner D, Belezai C, Girardeau-Montaut JP, Templier C, Gonnord H. A new method to determine laser damage threshold for thin diamond-like carbon films on silicon. *Diam Relat Mater* 2000;9:786–91.
- Asakura K, Yan J. Ultraprecision micro grooving on brass for surface wettability control. *Adv Mater Res* 2014;1017:489–94.
- Vermeeren V, Wenmackers S, Wagner P, Michiels L. DNA sensors with diamond as a promising alternative transducer material. *Sensors* 2009;9:5600–36.
- Bixler GD, Bhushan B. Bioinspired rice leaf and butterfly wing surface structures combining shark skin and lotus effects. *Soft Matter* 2012;8:11271.
- Cassie ABD, Baxter S. Wettability of porous surface. *Trans Faraday Society* 1940;40:546–51.
- Wenzel RN. Resistance of solid surfaces to wetting by water. *Ind Eng Chem* 1936;28:988–94.
- Bico J, Marzolin C, Quéré D. Pearl drops. *Europhys Lett* 1999;47:220–6.
- Chen Y, He B, Lee J, Patankar NA. Anisotropy in the wetting of rough surfaces. *J Colloid Interface Sci* 2005;281:458–64.
- Rahman MA, Jacobi AM. Comparison of frosting, defrosting and condensate retention characteristics of vertical parallel microgrooved and plain brass surfaces in forced convection condition. In: Meyer JP, editor. Proceedings of 8th International Conference on Heat Transfer, Fluid Mechanics and Thermodynamics. Mauritius: Pointe Aux Piments; 2011. p. 204–12.
- Ebert D, Bhushan B. Durable Lotus-effect surfaces with hierarchical structure using micro- and nanosized hydrophobic silica particles. *J Colloid Interface Sci* 2012;368:584–91.
- Zhang F, Low HY. Anisotropic wettability on imprinted hierarchical structures. *Langmuir* 2007;23:7793–8.